Colloids and Surfaces A: Physicochem. Eng. Aspects 382 (2011) 64–73

Contents lists available at ScienceDirect

Colloids and Surfaces A: Physicochemical and Engineering Aspects

journal homepage: www.elsevier.com/locate/colsurfa

A new device for assessing film stability in foams: Experiment and theory

M. Kostoglou, E. Georgiou, T.D. Karapantsios*

Department of Chemical Technology, School of Chemistry, Aristotle University, Univ. Box 116, 541 24 Thessaloniki, Greece

ARTICLE INFO

Article history:
Received 27 September 2010
Received in revised form
13 December 2010
Accepted 16 December 2010
Available online 23 December 2010

Keywords:
Foam stability
Coalescence
Surfactant stabilization
Liquid bridge
Thin film
Electrical resistance measurements

ABSTRACT

A new device is proposed for registering thin film drainage around a single foam bubble based on the increase of the electrical resistance of the draining film. Initially, a small bubble is expanded inside an electrically conductive liquid bridge that is formed between two vertically aligned metallic electrodes. Then the liquid of the bridge is withdrawn at a pre-selected flow rate until rupture of the bridge/bubble system while monitoring its electrical resistance across the electrodes. The present work reports results for liquid withdrawal rates between 20 and 200 μl/h which correspond to total drainage time between ~3 and ~25 min. Experiments are performed with aqueous solutions of SDS between 50 and 2000 ppm. A simple theoretical model is used to describe the evolution of the resistance of the global liquid bridge/bubble system. The model assumes a perfectly spherical bubble which affects the shape of the liquid bridge only as a volume constraint. A simple approach is employed for the computation of the electrical resistance of the system during the last stages of drainage where the thin film around the bubble gets gradually thinner and stretches until rupture. A detailed parametric study of the model is presented. The comparison between experimental and model results demonstrates the potential of the new device for the assessment of foam stability with respect to coalescence.

1. Introduction

Foams are structured gas/liquid fluids in which gas bubbles are separated by liquid layers that can be relatively thick (wet foams) or thin (dry foams). There is a vast literature devoted to fundamental aspects of foam formation and stability. Foams are destabilized through various mechanisms [1]. Drainage is a major foam destabilization mechanism referring to the flow of liquid relative to bubbles driven by gravity and capillary forces (the latter is known as marginal regeneration). In addition, foams coarsen because of diffusion of gas across films from small bubbles (high pressure) to large bubbles (low pressure) but also because interbubble films get thin, unstable and break. Both mechanisms result in the growth of the average bubble size.

Many detailed models can be found in literature on drainage [2]. During drainage a liquid-hold up profile is generated in the foam with increased liquid content along the flow. The liquid hold-up spatial profile corresponds to a spatial profile of the radius of curvature of the bubbles and, consequently, to the development of a pressure gradient (due to capillarity) which resists the drainage flow. The bubble size distribution is related to the capillary pressure and so it affects the drainage rate [3].

The bubble size distribution evolves towards larger sizes and the mechanism for this depends on the stability of the interbubble thin films existing in the foam. Some studies have tried to establish principles and criteria based on isolated foam films in order to understand the complex mechanisms of foam destabilization [4]. The stability of these films depends on the employed surfactant(s) and it is the result of two competing forces: capillary drainage of liquid towards Plateau borders and disjoining pressure [5]. In case of stable interbubble films, the bubble size evolution is chiefly due to Ostwald ripening i.e. gas transfer from the smaller to the larger bubbles due to their different internal pressure which induces different gas solubility [6,7]. In case of unstable interbubble films, the bubble size evolution occurs at a faster time scale and it is chiefly due to coalescence between neighboring bubbles as a result of interbubble thin film rupture [8]. In principle, the rupture rate of unstable films can be estimated from the evolution of the experimentally measured bubble size distributions at a specific location in the foam employing also the experimental information on the local liquid content distribution. In this way, the influence of the surfactant presence to the film rupture rate can be assessed. The above approach requires setting up and solving an inverse population balance for a very complicated problem (even for the direct problem very few attempts can be found in the literature) [9,10].

Here an alternative way is proposed for the assessment of a surfactant's influence on coalescence based on an innovative experimental process governed by the same physical laws as film rupture in a foam. The new process calls for the formation of a bubble

* Corresponding author.
E-mail address: karapant@chem.auth.gr (T.D. Karapantsios).

0927-7757/$ – see front matter © 2010 Elsevier B.V. All rights reserved.
doi:10.1016/j.colsurfa.2010.12.028

inside a small liquid bridge formed between two rigid rods. This configuration resembles the situation in a foam of a small bubble surrounded by segments of larger (equally sized) bubbles which are represented by the external surface of the bridge. The withdrawal of liquid from the bridge at a controlled flow rate generates drainage of the liquid layers between the small inner bubble and the outer bridge surface which is registered by electrical resistance measurements. It must be stressed that in this configuration no Plateau borders exist between the inner bubble and the outer bridge surface but instead there is an annular liquid layer with axially varying thickness, i.e. like a saddle, surrounding the inner bubble. This liquid layer gets progressively narrower in the axial direction becoming just a thin film near the bubble's equator and from that point on it progressively thickens again. This is a unique feature that allows examination of film drainage alone avoiding the complication of simultaneous drainage through Plateau borders. On this account, the new technique differs from other recent works that measure drainage in single Plateau borders [11,12]. Depending on the employed surfactant(s) but also on the liquid withdrawal rate one can examine the drainage of either stable or unstable interbubble films. Here, as a first step we examine the case of a surfactant creating unstable films regarding rupture (as determined by the disjoining pressure) but still being capable of reducing the rupture rate (by creating film elasticity). The use of the term *elasticity* (when without any further note) in the present work implies the combination of Gibbs and Marangoni elasticities.

The concept of this technique was inspired from our work on the behavior of small liquid bridges when varying their volume, length and contact characteristics with their end-supports [13–15]. By employing electrical resistance measurements we found that depending on experimental conditions a bridge could break either rapidly while still having a thick mid-height neck or slowly with the liquid at the neck forming a thin film that needs to stretch in order to snap.

Electrical resistance methods have been extensively employed for both understanding the conductive properties of foams and for the investigation of the initial expansion and subsequent stability of various foams. Working with multi-probe measuring systems Karapantsios and Papara [16] reviewed the critical design and operational aspects of electrical resistance techniques in measuring foaming properties. Electrodes geometry/arrangement and electric current excitation frequency were shown to be the most important parameters affecting the sensitivity and accuracy of measurements. In addition, a small but clear effect of bubble size on electrical measurements was presented. In a subsequent study, Papara et al. [17] examined how the diameter, wettability and shape of the container walls affect the liquid profile along a foam.

Despite the wealth of published electrical resistance measurements in foams, the use of such measurements to determine the stability of isolated thin films during drainage has been limited and has been chiefly focused on the liquid layer at the wall [18,19]. To our knowledge, there is no previous work dealing with electrical measurements of single thin films isolated between neighboring bubbles of a foam. In addition, the few other methods that have been developed for the study of isolated film drainage, e.g. interferometry, infrared spectroscopy, X-ray reflectivity [20–22] are rather complex and interpretation of measurements relies on models assuming specific film structures.

The structure of the present work is as follows: in the next section the experimental device, the procedure followed for the experiments and the corresponding conditions are described. Then the formulation of the corresponding theoretical problem, the sequence of assumptions and the numerical solution techniques are described in detail. Several indicative results for the behavior of the system under equilibrium conditions are presented. Finally, the theoretical results are compared to the experimental ones and a procedure for assessing the film stabilization capacity of surfactants using the new device is proposed.

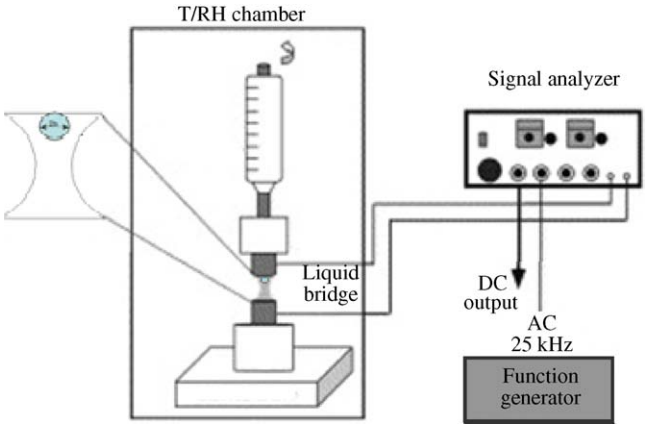

Fig. 1. Schematic of the experimental setup.

2. Experimental

The experimental setup is shown in Fig. 1. Liquid bridges are edge-pinned between the tips of two equal diameter solid rods which are aligned vertically. The upper rod is coupled with a precision cathetometer with a resolution of 5 μm/division. The cathetometer is used to adjust the separation distance between the rods (the lower rod is permanently fixed). Rods are constructed of copper which is an excellent electrical conductor. The free edges of the rods are carefully machined to be knife-edged circles with a radius $R = 1.6$ mm. The setup is placed inside a temperature/humidity regulated chamber to prevent evaporation of the bridge liquid. In this work, temperature is regulated at 30 ± 1 °C and relative humidity at $95 \pm 2\%$. The temperature of the liquid in the bridge is not measured directly in order to avoid intrusion and electrical interference with a sensor. The liquid temperature is assumed equal to the temperature of the nearby free surface of the lower rod which is measured by an ultra-thin (0.1 mm) surface thermocouple dressed with self-adhesive backing on one side to stick on the rod and insulation on the other side. This thermocouple is used for temperature control of the *T*/*H* regulated chamber.

The experiments are performed with pure deionized water (5.4 μS/cm at 25 °C) and sodium dodecyl sulfate (SDS) solutions. This particular surfactant is known for producing foams unstable with respect to coalescence [23]. Experiments are conducted using four concentrations of SDS (300, 600, 1000 and 2000 ppm) in deionized water. These concentrations are below the reported CMC value for 30 °C (~2500 ppm [24]). A small amount of NaCl (4×10^{-3} M) is added to the deionized water to yield the ionic strength that is met in applications where foams are produced from fresh (mineral) water (Table 1) but avoiding the fouling problems created by calcium and magnesium salts. This small concentration of salt does not affect interfacial properties. It must be stressed that the present electrical technique is fully functional down to ~10 μS/cm electrical conductivity. Equilibrium surface tension is measured by the

Table 1
Electrical conductivity and equilibrium surface tension of the solutions versus SDS concentration (at 30 °C).

	Concentration of SDS (ppm)				
	0	300	600	1000	2000
Electrical conductivity, mS/cm	0.55	0.62	0.69	0.81	1.05
Equilibrium surface tension, mN/m	71.3	56.2	51.8	44.7	33.7

Wilhelmy plate technique (TE2, Lauda). The surface tension of the solutions is presented in Table 1.

An ultra-precision microsyringe (10 μl, Hamilton) is used to deposit the liquid that forms the liquid bridges. Bridges of 20 μl pinned to the edge of the supporting rods are produced. This liquid volume is small enough to provide a bridge of approximately cylindrical shape when initially deposited between the rods. The cylindrical shape allows viewing the size of the bubble inside the bridge (see below) undistorted in the vertical direction. In addition, this liquid volume is large enough to offer easy operation and measuring convenience of the liquid bridge geometrical characteristics. Another ultra precision microsyringe (10 μl, Hamilton) driven slowly by a syringe pump (KD Scientific Inc., Model 100 series) is used to generate a small bubble inside the liquid bridge through a small hole (r = 0.15 mm) at the center of the surface of the upper rod. The rim of this hole is the contact line of the bubble with the upper rod during all times. This is so because, the metallic surface of the rods is highly wettable by the liquid especially in the presence of SDS.

Each experiment starts with forming a liquid bridge and a stable bubble (radius b = 0.6 mm) inside the bridge. Then, using a syringe pump (KD Scientific Inc., Model 100 series), liquid is drained off the bridge at a constant rate up to moment of rupture of the bridge. In this work, experiments are conducted using four nominal drainage rates: 20, 50, 100 and 200 μl/h.

During the experiments, the instantaneous apparent electrical conductance of the bridge is recorded and stored in a microcomputer. Data are acquired with a variable sampling frequency in the range 1–3 Hz. The conductance probe comprises of the two metallic rods serving as electrodes. An a.c. carrier voltage of 0.5 V (peak-to-peak) is applied across the probe at a frequency of 25 kHz in order to suppress undesirable electrode polarization and capacitive impedance. The response of the probe is fed to a special analyzer-demodulator. The analogue d.c. voltage output of the analyzer is converted to equivalent conductance K_{app} of the liquid between the electrodes using a calibration curve based on precision resistors. More details on these electrical measurements can be found in our previous work on liquid bridges [13–15]. At least three records are taken at all experimental conditions with good reproducibility. Pearson correlation coefficients among sampled curves are always above 0.97, whereas average instantaneous signal deviations are around 2%.

A video camera (EUROCAM, VC 5000) furnished with proper macro lenses is used to record at 25 fps the evolving shape of the liquid bridge during drainage. Image processing delivers several geometrical details of the bridge such as width of the neck, distance of the neck from the supporting rods, angle θ between the liquid and the surface of the rods etc. These data serve as shape parameters when solving the bridge descriptive equations (see below) but are not presented here due to space limitations. Further to the above, video images deliver the bubble shape inside the bridge when the bridge is initially cylindrical. In this case, lengths measured along the vertical direction can be trusted. The subsequent stability of the size of the bubble during the drainage experiments is monitored by a very sensitive differential pressure transducer (1 cm H_2O per volt, Honeywell) connected to the bubble via the hole in the upper rod. Although, the pressure in the bridge increases slightly during drainage because of the shape evolution of the bridge, this is not enough to affect the bubble size [13–15].

3. Theoretical analysis

3.1. Model formulation

The complete theoretical problem of the motion of the liquid bridge–bubble system during liquid withdrawal is extremely complicated involving a multitude of phenomena at several size and time scales. In principle the Navier–Stokes equations must be solved for the fluid simultaneously with the surfactant conservation equation. The adsorption–desorption process of the surfactant on the gas–fluid interfaces and its surface diffusion must be considered as boundary condition to the surfactant conservation equation. In addition, the normal stress and the tangential stress boundary conditions of the Navier–Stokes equations must be applied to the gas–fluid interfaces [25]. These conditions include surface tension gradients induced by non-uniformities of surfactant surface concentration leading to Marangoni effect [26]. Furthermore, a disjoining pressure effect must be considered as the film between bubble and liquid bridge interfaces becomes extremely thin. The system of the above equations consist a free boundary problem since the evolution of the shape of the gas–liquid interface is not defined but arises as part of the solution. The numerical solution of the complete problem is extremely difficult so a set of reasonable assumptions will be considered.

The first assumption is that the magnitude of the velocities in the flow field is relatively small with respect to the pressure terms in the normal stress boundary condition. In addition, convection ensures that the surface concentration of the surfactant is always uniform at its equilibrium values as the bridge's surface varies. The combination of the above two assumptions permits the decomposition of the original problem to two subproblems: the first subproblem stands for the evolution of the shape of the liquid bridge considering a quasi-steady equilibrium shape at every instant. This shape is dictated by a static equilibrium condition and the time value enters the problem through the remaining liquid volume. The second subproblem stands for the flow field in the evolving fluid domain defined by the first subproblem. In the present work, the first subproblem is of interest since the shape of the liquid bridge is the actually measured quantity from which the film stability information is inferred. This shape can be found by minimizing the following functional expression of the system shape which corresponds to the total energy of the system:

$$E = (\text{external surface energy}) + (\text{bubble's surface energy}) + (\text{potential energy induced by the gravitational field}) + (\text{thin film interaction energy})$$

The first three terms refer to the energy of the gas–liquid interfaces (bridge and bubble) and to the gravity force. The last term is the one related with the stability of the foams. The more this term offers to the stability of the bridge–bubble system the more stable will be the corresponding foam against rupture. This term is in general difficult to be quantified requiring a considerable theoretical and numerical effort due to the complicated interactions and forces that stabilizes the film. An alternative approach is suggested here: the film energy term is ignored for the computation of the shape of the bridge but its significance is estimated from the deviation between the theoretical calculations and the experimental measurements for the bridge shape evolution. It is noted here that the film energy term includes not only a static contribution (e.g. disjoining pressure) but a dynamic contribution (e.g. Gibbs–Marangoni elasticity associated to surfactants) as well. The assumption of an equilibrium concentration of surfactant made for the largest part of the bridge surface does not hold in the region of the very thin film near the bubble's equator. Macroscopic equilibrium properties such as the Gibbs elasticity of the bridge are taken into account as follows: a global mass balance for the surfactant is performed at each moment and the surfactant present to the system is shared between the surface (considering its evolving area) and bulk (evolving volume) employing the adsorption

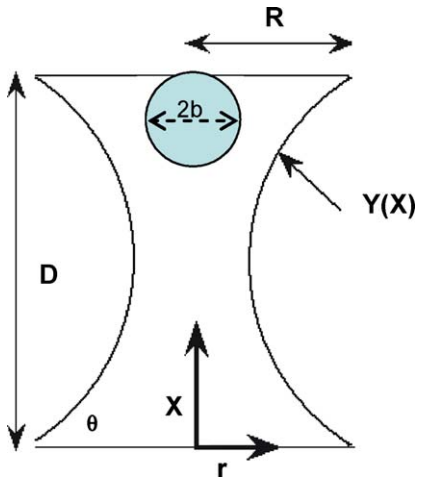

Fig. 2. Schematic of the liquid bridge–bubble system.

isotherm for the particular surfactant employed and the Gibbs equation.

Further simplification of the mathematical problem is based on the following assumptions justified by the present experimental observations: (i) the liquid wets completely the electrode's metallic surface (i.e. contact angle 0°) so the bubble touches the upper electrode at just one point. (ii) the bubble has a spherical shape. For the present experiments the radius of the bubble is smaller that the 1/3 of the length of the liquid bridge which means that the bubble Bond number is one order of magnitude smaller than the bridge Bond number (based on the bridge length). Therefore, it can be argued that the bubble does not deviate significantly from sphericity even if the shape of the bridge is affected by gravity. (iii) The bubble radius remains constant during drainage. As the liquid bridge shrinks the pressure in the bridge increases which may lead to a decrease of the radius of the bubble especially at the last stages of the drainage process. The bridge has two principal curvatures with opposite signs so its average curvature is much smaller than the average curvature of the bubble (having smaller dimensions than the bridge). This implies that the radius reduction of the bubble due to the increase of bridge pressure is small (as also confirmed by the experimental results) and at a first approximation can be ignored. According to the above assumptions the bubble retains always a spherical shape with a constant radius (equal to its initial value) which is considered as a parameter of the problem. The bubble surface energy term in the energy functional expression can be ignored and the bubble enters the mathematical problem for the bridge shape only as a volume constraint.

The geometry of the problem is shown in Fig. 2. The radius of the rods is R, the distance between the rods (length of liquid bridge) D, the radius of the bubble is b, X and r are the axial and radial coordinates respectively and $Y(X)$ is the function that describes the shape of the liquid bridge. In what follows all variables are made dimensionless by division with R. The bridge Bo number is defined as $\mathrm{Bo} = \rho g R^2/\gamma$ where ρ and γ are the density and surface tension of the liquid, respectively. The shape of the axisymmetric liquid bridge is given from the solution of the Young–Laplace equation [27]:

$$-\frac{d^2Y}{dX^2}\left(1+\left(\frac{dY}{dX}\right)^2\right)^{-3/2}+\frac{1}{Y}\left(1+\left(\frac{dY}{dX}\right)^2\right)^{-1/2}=H-\mathrm{Bo}X \quad (1)$$

For the purposes of the present work, H is a dummy parameter which must be found from the total volume constraint. The resulting non-linear boundary value problem exhibits pronounced sensitivity [28] to numerical accuracy so direct discretization approaches are not successful. The problem can be transformed to a system of ordinary differential equations using the arc length as independent variable [29] and then eliminating it reducing the number of equations from three to two. The governing equations are:

$$\frac{d\Phi}{dX}=\frac{H-\mathrm{Bo}X}{\sin(\Phi)}-\frac{1}{\Psi} \quad (2a)$$

$$\frac{dY}{dX}=\frac{1}{\tan(\Phi)} \quad (2b)$$

The boundary conditions are $Y(0) = Y(D) = 1$. The total volume of the liquid bridge (nondimensionalized with πR^3) is given as

$$V=\int_0^D Y^2(X)-U(b^2-(X-D+b)^2)dX \quad (3)$$

where the function U is defined as $U(x) = 0$ for $x < 0$ and $U(x) = x$ for $x \geq 0$.

Eq. (3) is written as a differential equation with respect to X and is added as a third equation to the system (2):

$$\frac{dv}{dX}=Y^2(X)-U(b^2-(X-D+b)^2) \quad (4)$$

with $v(0) = 0$ and $V = v(D)$.

For a given set of parameters D, b, V the system of equations ((2) and (4)) constitutes a boundary value problem consisting of three equations but four boundary conditions. The fourth boundary condition is employed to find the unknown value of H. The shooting method is used for the solution of the problem. A value for H and a value for $\Phi(0)$ are initially assumed. The system of equations is transformed now to an initial value problem. The numerical integration of the system is performed by using an explicit Runge–Kutta integrator with specified relative accuracy (a value of 10^{-5} is set) [30] and a self-adjusting time step. The integrator returns the values $v(D)$ and $Y(D)$ which in general are different than the required values V and 1, respectively. So, a new problem is set up: find the H and $\Phi(0)$ values that lead to $v(D) = V$ and $Y(D) = 1$. This problem is solved using the Newton–Raphson method with a numerically calculated Jacobian matrix. Unfortunately, the problem exhibits an excessive parametric sensitivity which means that the convergence of the Newton–Raphson iterations occurs only if the initial values for H and $\Phi(0)$ are very close to their converged values. To overcome this problem the following zero order continuation procedure is followed: initially a cylindrical liquid bridge ($V = D$, $\mathrm{Bo} = 0$) is considered. For the particular liquid bridge the values $H = 1$ and $\Phi(0) = \pi/2$ are known so the Newton–Raphson procedure tautotically converges. Then a spherical bubble is incrementally growing in the bridge up to the size of the bubble of the real problem. For each new bubble size the initial values for H and $\Phi(0)$ are the convergent values of the previous bubble size. Then the same strategy is followed for an incremental increase of the Bo number up to its real value. Finally, the volume of the bridge is increased or decreased step by step up to its value. At the end of the continuation procedure, a convergent solution for the initial bridge–bubble system under the experimental conditions is taken. Then the bridge volume is decreased (as it happens in the experiment) up to the rupture point. The rupture point (liquid volume) is defined as the liquid volume at which the Newton–Rapshson iterations cannot converge to a solution for the bridge shape. The identification of this point is more accurate as the volume reduction step decreases. The liquid volume can be transformed to time units through the drainage flowrate.

The potential distribution in the liquid bridge in case of an electrical potential difference between the rods is given by the solution

of the following Laplace equation [13–15]

$$\frac{1}{r}\frac{\theta}{\theta r}r\frac{\theta P}{\theta r}+\frac{\theta^2 P}{\theta X^2}=0$$

$$\text{in } [U(b^2-(X-D+b)^2)]^{0.5} < r < Y(X) \text{ and } 0 < X < D \quad (5)$$

where P is the electrical potential normalized to be 1 at the one rod and 0 at the other. The boundary conditions for the above equation are

(6a) $P = 1$ for $X = 0$ and $0 < r < 1$

(6b) $P = 0$ for $X = D$ and $0 < r < 1$

$$\left(\frac{\partial P}{\partial \vec{n}}\right)_{r=Y(X)}=0 \quad (6c)$$

$$\left(\frac{\partial P}{\partial \vec{n}}\right)_{r=[U(b^2-(X-D+b)^2)]^{0.5}}=0 \quad (6d)$$

where $\vec{n}$ is the unit normal vector. Having found the potential distribution in the bridge, the dimensionless conductance K can be computed from the relation

$$K_{app}=-2\int_0^1\left(\frac{\theta P}{\theta X}\right)_{X=0} r dr \quad (7)$$

The conductance is made dimensionless by division with $\pi\sigma R$ where σ is the specific electrical conductivity of the liquid. The above mathematical problem is quite similar to the extensively studied problem of heat transfer in fins [31]. Eq. (5) can be in general solved using typical numerical methods like finite elements, finite differences or even boundary elements but this procedure is not easy to be applied here given the complexity of the shape of the liquid domain (especially in the case of a thin film formation) and its time evolution. An alternative approach is to use the approximate solution used in the theory of heat transfer in fins which leads to

$$K_{app}=\left(\int_0^D [Y^2(X)-U(b^2-(X-D+b)^2))]^{-1}dX\right)^{-1} \quad (8)$$

This solution can be considered as a zero order term to a formal expansion of the problem with respect to the slope of the surface of the liquid domain [14]. Despite the fact that the expansion parameter (slope of the shape) takes large values for the case of the bubble, the approximate solution for the conductance is reasonably accurate for most of the cases as it will be shown in the next section.

3.2. Indicative theoretical results and discussion

The first step is to confirm the validity of the approximate expression (8) for the conductance in case of the sudden cross-section changes imposed by the presence of the bubble. A cylindrical liquid bridge for which $K_{app} = K_o = 1/D$ is considered as benchmark. A spherical bubble of radius b (it is reminded that all size variables are normalized by R) touching one side of the bridge (upper rod) is considered in the cylindrical domain. The Laplace equation (5) with no-flux boundary conditions is solved for the series of geometries resulting for several values of the bubble radius b. The numerical solution is performed using a commercial finite element code. The approximate expression for the particular case at hand takes the form:

$$K_{app}=\left(D-2b+\int_0^{2b}[1-b^2+(X-b)^2]^{-1}dX\right)^{-1} \quad (9)$$

from which conductance values are computed by a simple numerical integration. The approximate normalized conductance values

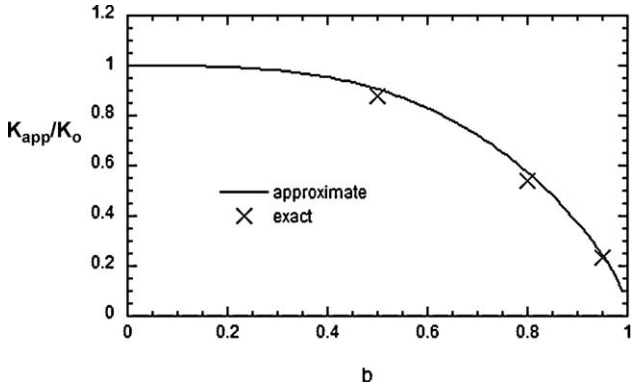

Fig. 3. Normalized conductance versus normalized bubble radius b for the benchmark geometry of a bubble inside a cylindrical liquid bridge. Comparison between approximate and exact solution of the Laplace equation.

K_{app}/K_o are shown versus bubble radius in Fig. 3. The corresponding values found using the finite element numerical technique for three values of b are shown in the figure for comparison purposes. The electrical potential contour plots (for $b = 0.5$ and $b = 0.8$) and the isopotential lines (for $b = 0.95$) are shown in Fig. 4. As it is shown in Fig. 3 the approximate technique leads to a slight over-prediction of the conductance for $b = 0.5$ and 0.8. This is compatible with the slight deviation of the potential field evolution from a direction parallel to the electrodes surface to a direction normal to the bubble's surface in Fig. 4a and b. What is really surprising is that the approximate technique is more accurate for the case of the large bubble with $b = 0.95$ despite the large deformation of the isopotential lines shown in Fig. 4c. The explanation is that in this case a thin film is formed near the equator of the bubble and almost all the contribution to the conductance is coming from this film region. But in this region the cross section variation is very low and the isopotential lines are parallel to the electrodes so the approximate theory is very accurate. The above case study confirms the validity of the approximate technique for the estimation of the conductance of the liquid bridge–bubble system.

All results refer to the experimental electrode radius ($R = 1.6$ mm) and to 20 μl liquid bridges. First, pure water is examined as the working liquid. The first issue is how the bubble modifies the external shape of the liquid bridge. The crucial factor is the influence of gravity. In the case of small influence of the gravity (this is realized by considering a short liquid bridge as shown in Fig. 5) the bubble is pushing the liquid bridge to expand outwards. A thin film between the outer bridge surface and the bubble does not appear in this case. As the bubble size increases

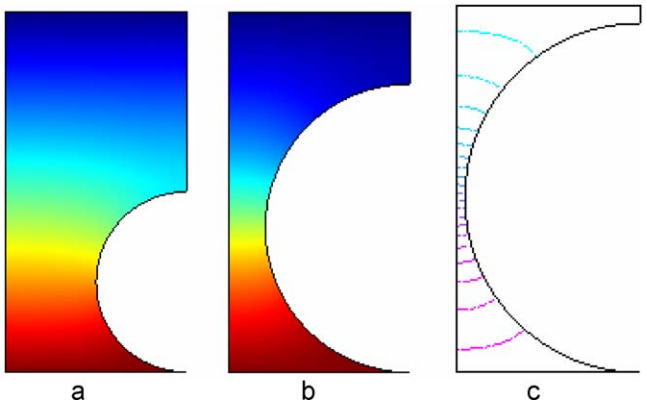

Fig. 4. Numerically computed electrical potential contours for $b = 0.5$ and 0.8 (cases (a) and (b), respectively) and isopotential lines for $b = 0.95$ (case (c)).

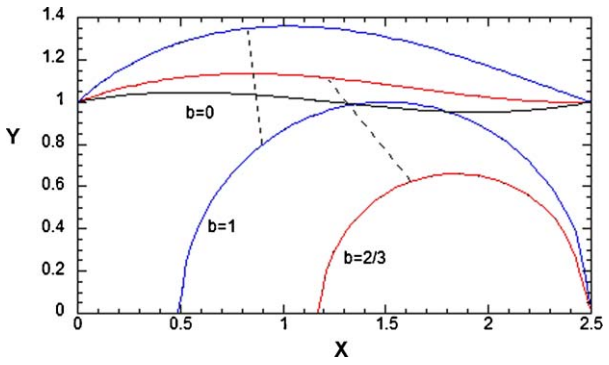

Fig. 5. Shape of the liquid bridge–bubble system for pure water as working liquid. The cases of no bubble ($b=0$) and $b=2/3$, $b=1$ are presented for a relatively short liquid bridge ($R=1.6$ mm, bridge length = 4 mm).

it will eventually reach the opposite electrode and then it will acquire a spherical section shape determined by its zero contact angle with the electrode surface. The bridge will accordingly attain an annular shape around the bubble until the moment of liquid leakage from the edge of the bottom electrode when the local angle overcomes a specific value. Theoretically, this will never happen for the assumed zero contact angle but in practice contact angle takes finite values.

The situation is completely different for the cases where gravity has a considerable influence on the shape of the liquid bridge. Such a case is realized by considering a long bridge in Fig. 6 as it is evident from the highly asymmetric bridge shape in the absence of a bubble ($b=0$). In this case a thin film is created between the bridge and the bubble as the bubble size increases leading to the destruction of the system at the moment of film rupture. So, the effect of gravity is crucial for the structure of the bridge–bubble system.

The effect of Bond number on the conductance of the liquid bridge–bubble system is studied next. The curves of the conductance K_{app} against the size of the bubble for the base case presented in Fig. 6 and for two more values of the Bond number are presented in Fig. 7. The value of K_{app} for the cylindrical bridge is $1/D = 1/3.5 = 0.285$. As it is shown the effect of gravity on $K_{app}(b=0)$ is negligible for $Bo < Bo_w/2$ (where the subscript w denotes water). The effect of the presence of a bubble on the conductance is practically zero for $b<0.4$ but as b increases further and a film is created between the bubble and the external surface of the bridge, K_{app} is getting more and more sensitive to b. If the Bond number is large enough the bubble grows up to the rupture of the bridge. Larger Bond numbers leads to rupture at smaller bubble size. For Bond number values smaller than a critical number, film rupture theoretically does not occur but the destruction of the system

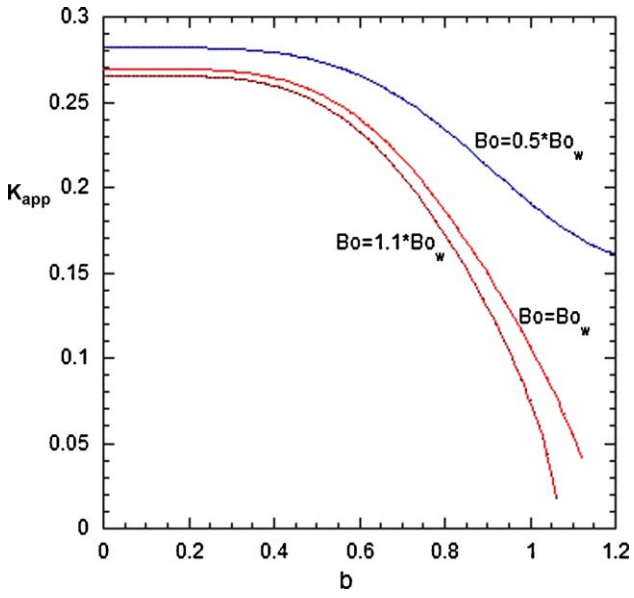

Fig. 7. Liquid bridge apparent conductance versus normalized bubble size for long bridge ($D=3.5$) and three values of Bond number (shown in relation to the Bond number corresponding to pure water, Bo_w).

appears as leakage of liquid from the bottom edges as described above.

The evolution of the liquid bridge shape during drainage (reduction of liquid volume) in the presence of a bubble of constant size is shown in Figs. 8 and 9 for a relatively small ($b=0.5$) and a relatively large bubble ($b=0.9$) respectively. There is a critical value for the radius of the bubble (for each set of the problem parameters). For a bubble smaller than the critical radius, bridge rupture occurs at the neck as is the case in the absence of a bubble. Surprisingly, the rupture occurs at a smaller liquid volume than in the absence of bubble [14] which means that the bubble stabilizes in some sense the bridge against rupture. This happens by preventing the thinning of the neck of the bridge. On the other hand, when a bubble is larger than the critical size, a thin film is created between the bubble and the bridge which gets constantly thinner during drainage until its disappearance. This happens at a volume larger than the rupture volume in the absence of bubble [14] so in this case the bubble destabilizes the bridge.

The dependence of K_{app} on the liquid volume for two values of the bridge length and two values of the bubble radius is shown in Fig. 10 for pure water as liquid. For a specific length of the liquid bridge rupture occurs at smaller liquid volume as the bubble radius becomes smaller. In general, the liquid volume at rupture is

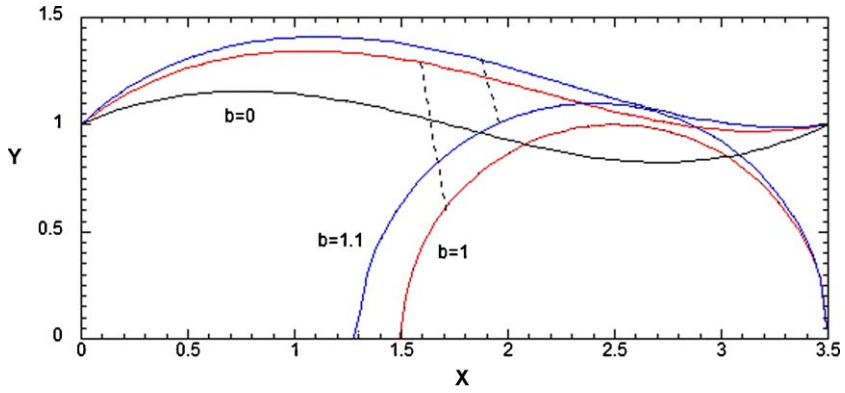

Fig. 6. Shape of the liquid bridge–bubble system for pure water as working liquid. The cases of no bubble ($b=0$) and $b=2/3$, $b=1$ are presented for a long liquid bridge ($R=1.6$ mm, bridge length = 5.6 mm).

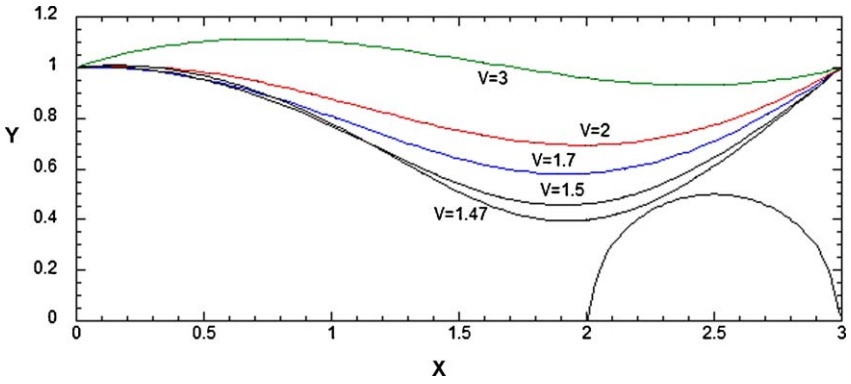

Fig. 8. Evolution of the liquid bridge shape when its volume is reduced due to drainage for pure water as working liquid. Case of a relatively small bubble leading to bridge neck rupture ($b = 0.5$, $V = 20$ μl, $R = 1.6$ mm).

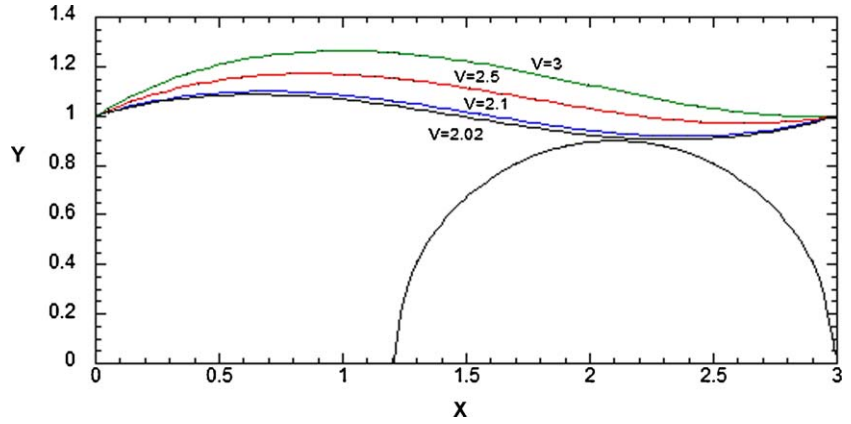

Fig. 9. Evolution of the liquid bridge shape when its volume is reduced due to drainage for pure water as working liquid. Case of a relatively large bubble leading to thin film rupture ($b = 0.9$, $V = 20$ μl, $R = 1.6$ mm).

smaller as the distance between the rods becomes smaller and the effect of gravity decreases. For the larger bubble size the rupture volumes are larger but the K_{app} curves reach (very abruptly) the value $K_{app} = 0$ (thin film disappearance). In case of smaller bubbles the rupture volume is smaller but K_{app} takes a finite value K_{rup} at the rupture point (neck rupture). Despite how large is the slop of the K_{app}–V curve in the film rupture case there is a fundamental difference between the two rupture modes: values $K_{app} < K_{rup}$ are not accessible in case of neck rupture mode in contrast to the film rupture mode where K_{app} passes (very abruptly) through all values down to $K_{app} = 0$.

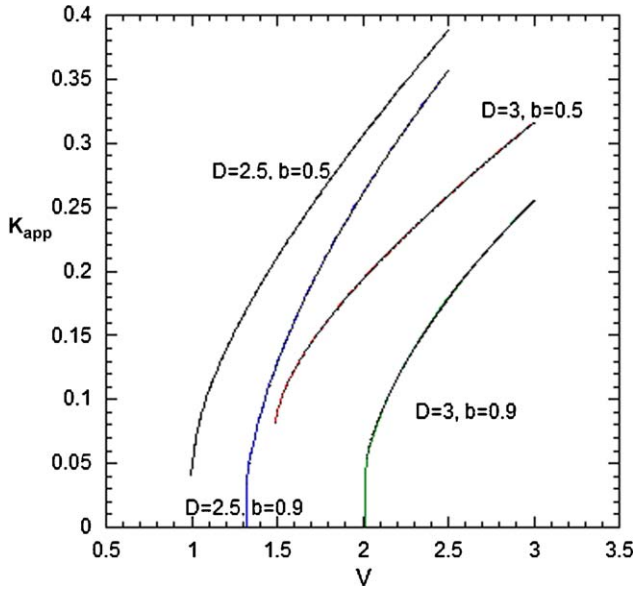

Fig. 10. Relation of the apparent conductance to liquid volume for the liquid bridge–bubble system (pure water as liquid, $V = 20$ μl, $R = 1.6$ mm and several combinations of D and b).

4. Experimental results – comparison with theory

The experimental curves of the evolution of the ratio K_{app}/K_o (K_o is the initial value of K_{app}) with respect to time are shown in Figs. 11–13 for the cases of no surfactant, 600 ppm and 2000 ppm of surfactant, respectively. In each figure four curves are presented corresponding to the examined four withdrawal rates. The theoretical curves are computed using the geometric parameters and the surface tension values corresponding to each experiment. The bridge volume which is the evolution parameter of the aforementioned algorithm is transformed to time using the nominal withdrawal rate of each experiment. The theoretical curves are also shown in Figs. 11–13 for comparison with the experimental curves. Although the time scales of theoretical and experimental curves practically coincide an important deviation is evident in all cases. The theoretical decrease rate of conductance is almost constant but the experimental one shows an increasing trend with time. This deviation cannot be due to the surfactant dynamics which has been ignored since it appears even for the no surfactant case. Also it cannot be due to the approximate nature of the solution of the electrical field problem since this solution is more accurate as the liquid bridge shape is closer to the cylinder. Furthermore, accord-

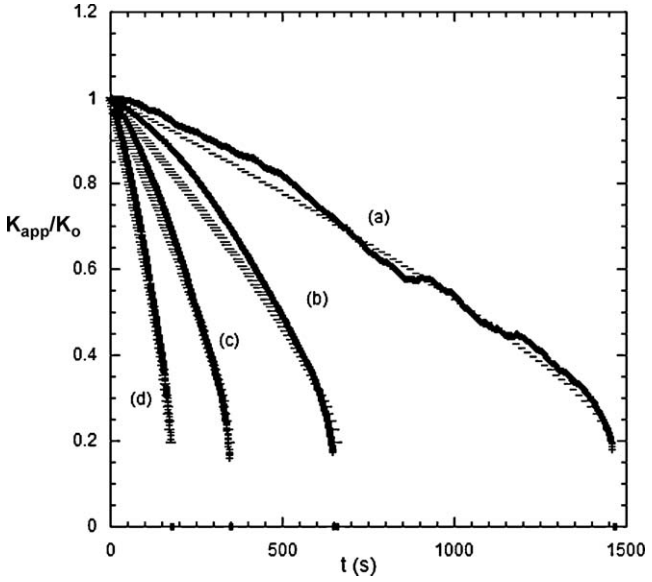

Fig. 11. Evolution curves of the normalized apparent conductance for pure water. The continuous lines display experimental results and the dashes the theoretical results. Drainage rates (a) 20 μl/h, (b) 50 μl/h, (c) 100 μl/h and (d) 200 μl/h.

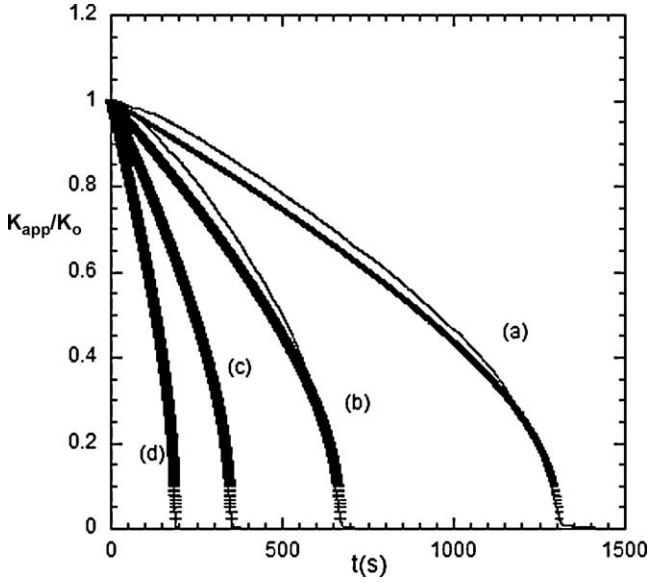

Fig. 13. Evolution curves of the normalized apparent conductance for solutions with 2000 ppm SDS. The continuous lines display experimental results and the dashes the theoretical results. Drainage rates (a) 20 μl/h, (b) 50 μl/h, (c) 100 μl/h and (d) 200 μl/h.

ing to the figures the deviation is larger for moderately distorted liquid bridges and it is reduced as the bridge distortion increases.

In order to have a clearer view of the deviations between theory and experiment the case of liquid withdrawal from a bridge having an initial cylindrical shape in the absence of bubble and surfactant is studied both theoretically and experimentally. In this particular case an exact solution of the conductance problem at least for the first stages of withdrawal is available through the domain perturbation approach. The well-defined (without assumptions) solution of the problem is $K_{app}/K_o = 1 - qt/V_o$ (q is the volumetric flow rate and V_o the initial liquid volume). The numerical and experimental curves are presented in Fig. 14. The numerical result shows a linear decrease with slope q/V_o which confirms the validity of the proposed algorithm. On the other hand, the same pattern that was observed in the previous cases is observed also for these experimental curves. The study of this simple case suggests clearly that the experimental withdrawal rate is not constant but increases with time. The variation of the withdrawal rate may be attributed to an ill-functioning syringe pump that was realized only after the end of the experimental campaign and the comparisons with theoretical predictions. However, this deviation between theoretical and experimental curves is not a problem since the experimental withdrawal rate can be estimated by matching the theoretical to experimental curves. As it will be shown below the thin film formation which is the focus of the present technique is not influenced by this matching procedure.

Regarding the last part of the conductance curves the following observations are made: the surfactant acts in two ways in the

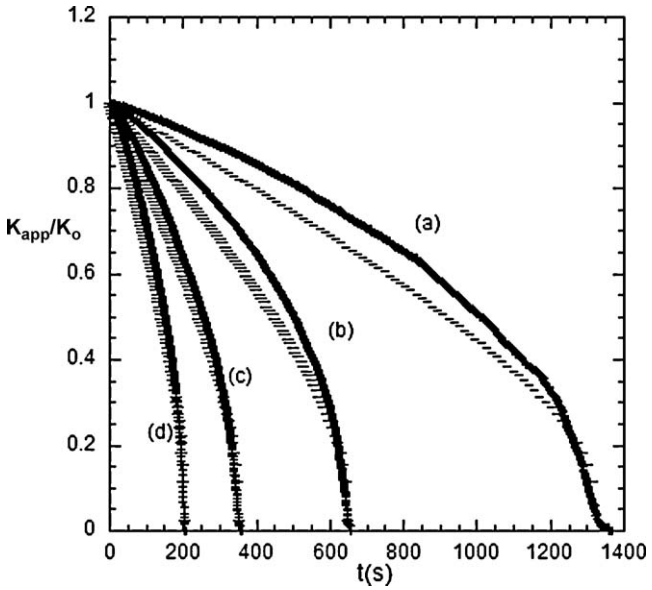

Fig. 12. Evolution curves of the normalized apparent conductance for solutions with 600 ppm SDS. The continuous lines display experimental results and the dashes the theoretical results. Drainage rates (a) 20 μl/h, (b) 50 μl/h, (c) 100 μl/h and (d) 200 μl/h.

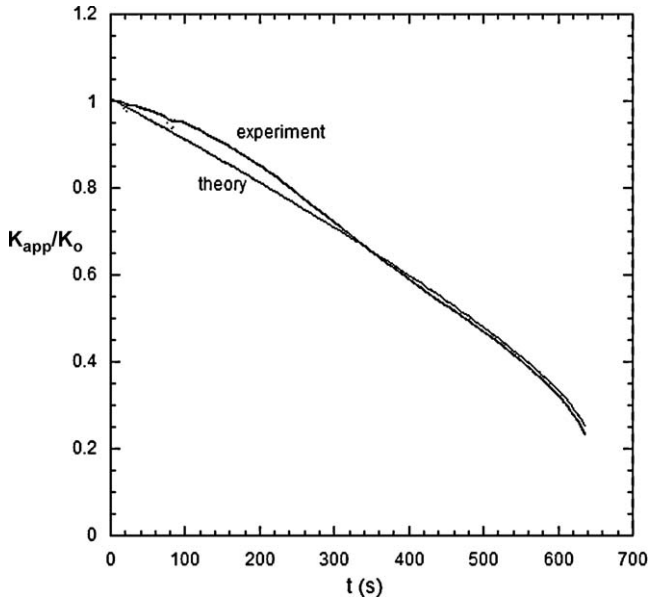

Fig. 14. Comparison of experimental and theoretical normalized apparent conductance evolution curves in the absence of bubble and surfactant (drainage flow rate 50 μl/h).

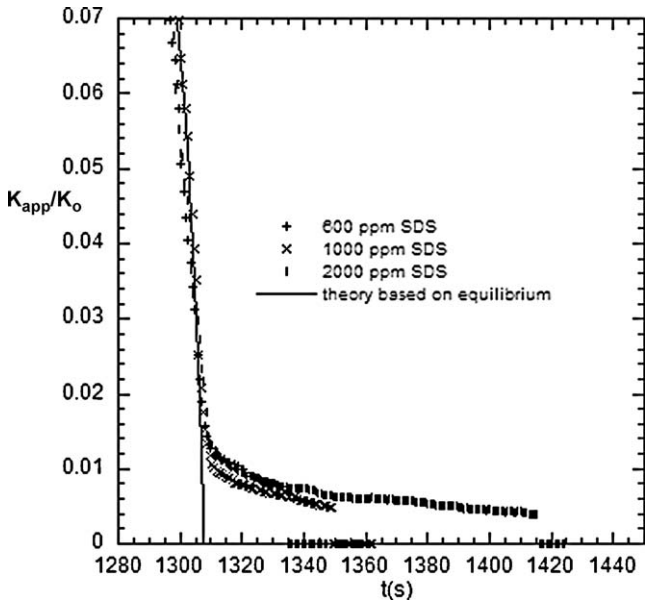

Fig. 15. Evolution of the normalized apparent conductance during the last stages of drainage of a liquid bridge where thinning of the film between the bubble and the external surface of the bridge is evidenced. The curves correspond to the lowest drainage rate examined (20 μl/h) and three surfactant concentrations.

process: (i) by reducing the equilibrium surface tension and (ii) by stabilizing the resulting thin film through the Gibbs elasticity. In the absence of surfactant the bridge breaks at its neck before the formation of a thin film. As the SDS concentration increases to 300 ppm the surface tension decreases but still the bridge breaks at the neck (finite film thickness at the rupture point). This case is not shown due to space limitations. Apparently, there is a threshold surface tension (depending on the geometric parameters) at which a transition takes place from the neck rupture to the film rupture in accordance with the theory which ignores surfactant dynamics. This assumption, however, does not hold for the case of a thin film between the bubble and the bridge surface where the non-uniformity of surfactant concentration creates Marangoni

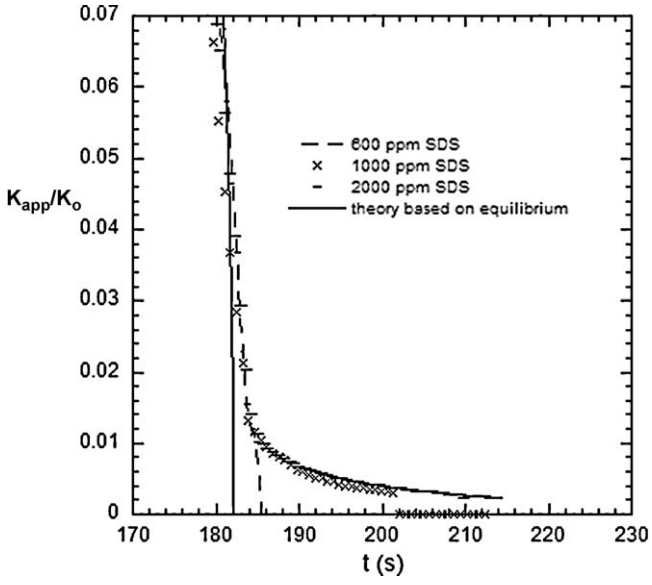

Fig. 16. Evolution of the normalized apparent conductance during the last stages of drainage of a liquid bridge where thinning of the film between the bubble and the external surface of the bridge is evidenced. The curves correspond to the highest drainage rate examined (200 μl/h) and three surfactant concentrations.

Table 2
Rupture time t_{rup} (s) versus drainage rate and SDS concentration.

	Flow rate (μl/h)			
	20	50	100	200
SDS concentration (ppm)				
600	22	9	4	2
1000	37	17	15	17
2000	104	42	28	28

convection which prevents further thinning of the thin film. So, when the theoretical model predicts the creation of a film and its fast thinning until its disappearance, in practice Gibbs–Marangoni elasticity inhibits the thinning beyond some thickness.

The conductance–time curves for three concentrations of SDS and for the smallest and largest examined drainage rates are shown in Figs. 15 and 16, respectively. Time has been shifted appropriately in order the curves to match each other far from the conductance elimination point. The theoretical curves based on the equilibrium properties are also shown indicating a fast film disappearance. The difference between the equilibrium curves and the experimental curves is due solely to the dynamic film stabilization properties of the surfactant. Although the direct observation of the film structure is not feasible the following seems to be the most probable scenario: during the thinning of the film between the bubble and the bridge, the film elasticity appears at the position of the smallest thickness where the film is stabilized and no further thinning occurs. Higher surfactant concentrations lead to the appearance of elasticity at thicker films. Then the area of the film is extended along the bubble surface. So, the gradual reduction of the K_{app}/K_o curve at this last stage of drainage is not due to the film thinning but to the elongation of the surfactant stabilized thin film. The current electrical technique cannot resolve simultaneously the film thickness and the film length. Nevertheless, according to the described view of the film structure and employing the lowest measured value of conductance, an approximate estimation of the stabilized film thickness is possible. Considering that the maximum film length is of the order of the bubble radius a conductance analysis leads to an estimation of the film thickness around 1 μm. This is a thick film whose rupture is not related to the usual combination of capillary forces-disjoining pressure assumed to determine the stability of foam films but can be ascribed to the combination of mechanical vibrations and elasticity [9].

Unfortunately, the film thickness at which Gibbs stabilization begins is not very sensitive to process parameters and given the experimental uncertainty cannot be used as a measure of the stabilization properties of the surfactant. On the other hand, the time of the final film rupture depends strongly on the surfactant concentration. The rupture of the film is due to the diffusion of surfactant along the film restoring the equilibrium surface tension of the film and vanishing the Gibbs–Marangoni elasticity. So, a measure of the film stabilization capacity of the surfactant is the time span between the instant of film creation and the instant of film rupture which for simplicity is called *rupture time*, t_{rup}. In order to avoid theoretical calculations to derive the instant of film creation, *rupture time* can be roughly assumed as the interval between the time designated by extrapolating linearly the sharply decreasing part of the conductance curve before the large slope variation associated to film stabilization, and the time where conductance falls to zero value. The rupture time is of course a function of the surfactant concentration and of the driving force for rupture (drainage rate). Table 2 displays rupture times estimated from the present experiments.

As expected, the rupture time t_{rup} increases when the surfactant concentration increases and the drainage rate decreases. For the case of 1000 and 2000 ppm of SDS a plateau appears for flow

rates larger than 50 μl/h. It is speculated that if larger bubbles would have been employed in the experiments the plateau might have appeared at larger flow rates since the film could have been extended further before rupture. However, much larger bubbles are rather unrealistic for foams of practical significance. Instead, one should turn his attention to drainage rates lower than 20 μl/h. The rupture time includes the effect of the resistance to film thinning (elasticity), film elongation, surfactant diffusion from the bulk through the film and the rupture driving force. Independent interpretation of these phenomena is not possible but since similar phenomena appear in wet foams t_{rup} may be an important measure to assess the effect of a surfactant on the coalescence rate of wet foams. Correlation between t_{rup} and coalescence rates estimated by solving the inverse population balance for the evolution of bubble size distributions in foams will be dealt with in the future using several surfactants. It is noted that the approach followed here is based on the idea of acceleration of the phenomena occurring in real foams in order to have a fast assessment of them. The acceleration idea has been tried before directly on foams by replacing the slow gravity induced drainage with fast drainage induced by applying a large pressure difference. In that case the phenomena of drainage and coalescence can be independently assessed [32,33]. In a similar fashion, the approach proposed in the present work isolates the phenomenon of coalescence whereas in real foams drainage and coalescence phenomena are fully coupled.

5. Conclusions

A new technique is proposed in the present work for the assessment of surfactants stabilizing foam bubbles against coalescence. This technique calls for recording the evolution of electrical conductance during forced drainage of liquid from a liquid bridge that contains a bubble. The thin liquid film created between the bridge and the bubble serves as an indicator for the behavior of the corresponding films in the foam. A theoretical framework is developed and after a sequence of assumptions, solutions for the equilibrium case became possible. By comparing the theoretical and experimental results the dynamic effect of stabilization of the film by the surfactant against rupture (delay of rupture time) is identified. A set of experiments were performed using SDS at various concentrations (below CMC) and it is found that the system (bridge geometry, liquid quantity, surfactant concentration) must be in a region which allows the formation of a thin film. Being in such a region the effect of surfactant can be assigned to a single parameter, namely, the rupture time. It is believed that this time is correlated with the coalescence rate of films in the foam. Such correlations will become the subject of subsequent research.

Acknowledgements

Financial support by the European Space Agency through the project FASES (ESA-AO-2004-PCP-109/ELIPS-2) is gratefully acknowledged. This work is conducted under the umbrella of the COST P21 action: Physics of Droplets.

References

[1] C. Stubenrauch, B.R. Blomqvist, Foam films, foams and surface rheology of nonionic surfactants: amphiphilic block copolymers compared with low molecular weight surfactants, in: T.F. Tardos (Ed.), Colloid Stability: The Role of Surface Forces I, Wiley, Weinheim, 2007.
[2] S.A. Koehler, H.A. Stone, M.P. Brenner, J. Eggers, Dynamics of foam drainage, Phys. Rev. E 58 (1998) 2097–2106.
[3] A. Britan, M. Liverts, G. Ben-Dor, S.A. Koehler, N. Bennani, The effect of fine particles on the drainage and coarsening of foam, Colloid Surf. A: Physicochem. Eng. Aspects 344 (2009) 15–23.
[4] G. Narsimhan, Ruckenstein Structure, drainage and coalescence of foams and concentrated emulsions, in: R.K. Prudhomme, S.A. Khan (Eds.), Foams: Theory Measurements and Applications, 1995.
[5] R.H. Yoon, L. Wang, Hydrophobic forces in foam films, in: T.F. Tardos (Ed.), Colloid Stability: The Role of Surface Forces I, Wiley, Weinheim, 2007.
[6] A. Monsalve, R.S. Schechter, The stability of foams dependence of observation on the bubble size distribution, J. Colloid Interface Sci. 97 (1984) 327–335.
[7] S.A. Magrabi, B.Z. Dlugogorski, G.J. Jameson, Bubble size distribution and coarsening of aqueous foams, Chem. Eng. Sci. 54 (1999) 4007–4022.
[8] A.V. Nguyen, H.J. Schulze, Colloidal Science of Flotation, Marcel Dekker, New York, 2004.
[9] A. Bhakta, E. Ruckestein, Drainage and collapse in standing foams, in: S. Hartland (Ed.), Surface and Interfacial Tension: Measurement, Theory and Applications, Marcel Dekker, New York, 2004.
[10] A. Bhakta, E. Ruckestein, Decay of standing foams: drainage, coalescence and collapse, Adv. Colloid Interface Sci. 70 (1997) 1–124.
[11] O. Pitois, C. Fritz, M. Vignes-Adler, Hydrodynamic resistance of a single foam channel, Coll. Surf. A: Physicochem. Eng. Aspects 261 (2005) 109–114.
[12] O. Pitois, C. Fritz, M. Vignes-Adler, Liquid drainage through aqueous foam: study of the flow on the bubble scale, J. Colloid Interface Sci. 282 (2005) 458–465.
[13] M. Kostoglou, T.D. Karapantsios, A new method for the characterization of electrically conducting liquid bridges, J. Colloid Interface Sci. 227 (2000) 282–290.
[14] T.D. Karapantsios, M. Kostoglou, A conductance study of reducing volume liquid bridges, J. Colloid Interface Sci. 255 (2002) 177–188.
[15] S. Evgenidis, M. Kostoglou, T.D. Karapantsios, Electrical conductance study of θ-liquid bridges, J. Colloid Interface Sci. 302 (2006) 597–604.
[16] T.D. Karapantsios, M. Papara, On the design of electrical conductance probes for foam drainage applications. Assessment of ring electrodes performance and bubble size effects on measurements, Colloid Surf. A 323 (2008) 139–148.
[17] M. Papara, X. Zabulis, T.D. Karapantsios, Container effects on the free drainage of wet foams, Chem. Eng. Sci. 64 (2009) 1404–1415.
[18] M. Barigou, F. Davidson, Soap film drainage: theory and experiment, Chem. Eng. Sci. 49 (1994) 1807–1819.
[19] B. Fournel, H. Lemonnier, J. Pouvreau, Foam drainage characterization by using impedance methods, in: 3rd Symposium on Two-Phase Modelling and Experimentation, Pisa, 22–24 September, 2004.
[20] K.J. Mysels, K. Shinoda, Frankel Soap Films: Studies of Their Thinning and a Bibliography, Pergamon, New York, 1959.
[21] D.C. Clark, R. Dann, A.R. Mackie, J. Mingins, A.C. Pinder, P.W. Purdy, E.J. Russel, L.J. Smith, D.R. Wilson, Surface diffusion in sodium dodecyl sulfate-stabilized thin liquid films, J. Colloid Interface Sci. 138 (1990) 195–206.
[22] T. Yamanaka, T. Tano, O. Kamegaya, D. Exerowa, R.D. Cohen, Effect of metal-ions on the equilibrium thicknesses of foam films stabilized by lysophosphatidycholine as studied by FT-IR spectroscopy, Langmuir 10 (1994) 1871–1876.
[23] E. Mileva, P. Tchoukov, Surfactant nanostructures in foam films, in: T.F. Tardos (Ed.), Colloid Stability: The Role of Surface Forces I, Wiley, Weiheim, 2007.
[24] S.S. Shah, N.U. Jamroz, Q.M. Sharif, Micellization parameters and electrostatic interactions in micellar solution of sodium dodecyl sulfate (SDS) at different temperatures, Colloid. Surf. A 178 (2001) 199–206.
[25] W.M. Deen, Analysis of Transport Phenomena, Oxford University Press, New York, 1998.
[26] J. Lyklema, Fundamentals of Interface and Colloid Science, Volume V: Soft Colloids, Elsevier, Amsterdam, 2005.
[27] J.A.N. Zasadzinski, J.B. Sweeney, H.T. Davis, L.E. Scriven, Finite elements calculations of fluid menisci and thin films in a model porous media, J. Colloid Interface Sci. 119 (1987) 108–116.
[28] C. Pozrikidis, Introduction to Theoretical and Computational Fluid Dynamics, Oxford University Press, New York, 1997.
[29] D.N. Mazzone, G.I. Tardos, R. Pfeffer, The effect of gravity on the shape and strength of a liquid bridge between two spheres, J. Colloid Interface Sci. 113 (1986) 544–556.
[30] M.D. Michailov, M.N. Özisik, Unified Analysis and Solutions of Heat and Mass Diffusion, Wiley, New York, 1984.
[31] W.H. Press, S.A. Teukolsky, W.T. Vetterling, B.P. Flannery, Numerical Recipes, Cambridge University Press, New York, 1992.
[32] K. Khristov, D. Exerowa, K. Malysa, Surfactant foaming: new concepts and perspectives on the basis of model studies, in: Proceedings Eurofoam 2000, Delft, The Netherlands, 2000, pp. 21–31.
[33] K. Khristov, D. Exerowa, L. Christov, A. Makievski, R. Miller, Foam analyzer: an instrument based on the foam pressure drop technique, Rev. Sci. Instrum. 75 (2004) 4797–4803.